Tumor Suppressor INK4: Quantitative Structure−Function Analyses of $p18^{INK4C}$ as an Inhibitor of Cyclin-Dependent Kinase 4†

Junan Li,‡ Ming Jye Poi,§ Dongyan Qin,§ Thomas L. Selby,|| In-Ja Byeon,⊥ and Ming-Daw Tsai*,‡,§,||,⊥

Departments of Biochemistry and Chemistry, Ohio State Biochemistry Program, and Campus Chemical Instrument Center, The Ohio State University, Columbus, Ohio 43210

Received June 4, 1999; Revised Manuscript Received November 2, 1999

ABSTRACT: We report the first detailed structure−function analyses of $p18^{INK4C}$ (p18), which is a homologue of the important tumor suppressor $p16^{INK4A}$ (p16). Twenty-four mutants were designed rationally. The global conformations of the mutants were characterized by NMR, while the function was assayed by inhibition of cyclin-dependent kinase 4 (CDK4). Most of these mutants have unperturbed global structures, thus the changes in their inhibitory abilities can be attributed to the mutated residues. The important results are summarized as follows: (a) some residues at loops 1 and 2, but not 3, are important for the inhibitory function of p18, similar to the results for p16; (b) two residues at the first helix-turn-helix motif and two at the third are important for inhibition; (c) while the results generally agree with the prediction based on the crystal structures of p16−CDK6 and p19−CDK6 binary complexes, there are significant differences in a few residues, suggesting that the interactions in the binary complexes may not accurately represent the interactions in the ternary complexes (in the presence of cyclin D2); (d) most importantly, the extra loop of p18 appears to contribute to the function of p18, even though the crystal structure of the $p19^{INK4D}$−CDK6 complex indicates no interactions involving this loop; (e) detailed analyses of the crystal structures and the functional results suggest that there are notable differences in the interactions between different members of the INK4 family and CDKs.

INK4[1] proteins are a group of ankyrin repeat-containing proteins, which specifically bind to and inactivate cyclin-dependent kinases 4 and 6 (*1*−*6*). Currently, there are four known members of the INK4 family, $p16^{INK4A}$, $p15^{INK4B}$, $p18^{INK4C}$, and $p19^{INK4D}$ (which are abbreviated as p16, p15, p18, and p19, respectively, in this paper) (*7*−*13*). While p15 and p16 consist of four ankyrin repeats (ankyrin I−IV), p18 and p19 have five (ankyrin I−V). An ankyrin repeat is a motif of about 34 amino acid residues and is present in a large number of proteins. Ankyrin repeats exist in groups of four or more and are often involved in protein−protein interaction (*14*, *15*). Since 1997, the tertiary structures of p19 (*16*), p18 (*17*, *18*), p16 (*19*), and p15 (*20*) have been reported. The structures of INK4 proteins are linear arrays of repeating helix-turn-helix (H-T-H) units linked by relatively flexible loops (*15*, *16*, *19*, *20*). Figure 1 shows the correlation between p16, p15, p18, and p19 in terms of residue numbers and the locations of helices (e.g., helix IA stands for the first helix of the first ankyrin) and loops (e.g., loop 1 stands for the first loop, connecting ankyrin I and ankyrin II). Another major advance in the field is the recent solution of the crystal structures of p16−CDK6 (*21*) and p19−CDK6 (*22*) binary complexes. In the crystal structure of the p16−CDK6 complex, p16 binds to one side of the catalytic cleft of CDK6, opposite the cyclin-binding site. The concave surface of p16 contacts the N lobe of CDK6, while the loops between neighboring ankyrin repeats interact with the C lobe. As a result, the interactions between p16 and CDK6 involve multiple regions in both proteins. Most of the interacting residues in p16 are located in the first two loops and the most conserved ankyrin repeats II and III. However, contrary to what one might expect, the solution structures of p16 (*19*, *20*) and p19 (*16*) are virtually unchanged upon binding to CDK6 (*21*, *22*).

Despite the extensive structural and functional studies, we are still far from a complete understanding of the mechanism of inhibition by INK4 proteins for the following reasons: First, the biologically relevant complex is likely to be the INK4/CDK/cyclin D ternary complex, not the INK4−CDK binary complex. Although the existence of the ternary complex in vivo remains to be firmly established, it has been

† This work was supported by NIH Grant CA69472, and by American Cancer Society Grant IRG 16-33. The DMX-600 NMR spectrometer used was funded in part by NIH Grant RR08299 and NSF Grant BIR-9221639. The DRX-800 NMR spectrometer was funded by Ohio Board of Regents. This is paper 5 in the series Tumor Suppressor INK4; for paper 4, see reference *31*.

‡ Department of Biochemistry.

§ Ohio State Biochemistry Program.

|| Department of Chemistry.

⊥ Campus Chemical Instrument Center.

* To whom correspondence should be addressed at the Department of Chemistry, The Ohio State University, 100 West 18th Avenue, Columbus, OH 43210-1185. Telephone: 614-292-3080. Fax: 614-292-1532. E-mail: Tsai.7@osu.edu.

[1] Abbreviations: CD, circular dichroism; CDK, cyclin-dependent kinase; DTT, dithiothreitol; EDTA, ethylenediamine tetraacetic acid; GST, glutathione-S-transferase; HEPES, *N*-[2-hydroxyethyl] piperazine-*N*′-[2-ethane-sulfonic acid]; INK4, inhibitor of CDK4; IPTG, isopropyl-*β*-D-thiogalactoside; pRb, retinoblastoma gene product; SDS-PAGE, sodium dodecyl sulfate polyacrylamide gel electrophoresis; WT, wild-type.

10.1021/bi991281u CCC: $19.00
Published on Web 01/04/2000

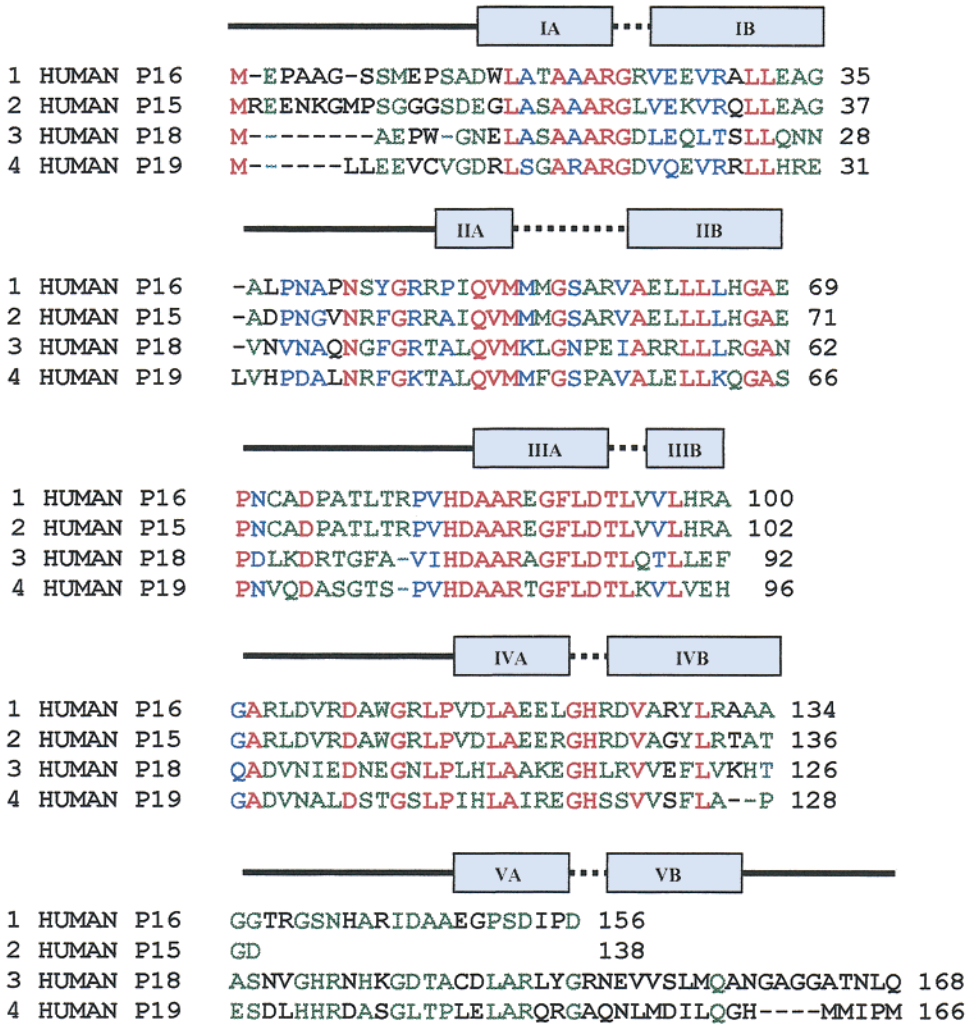

FIGURE 1: Sequence comparisons among INK4 proteins and the secondary structure of $p16^{INK4A}$. Antheproct program was used to do this assignment. Residues with different identities are shown in different colors: 100%, red; more than 75%, blue; more than 50%, green; less than 50%, black.

shown that in an in vitro system containing preassembled CDK4/6−cyclin D complexes, the binding of INK4 proteins does not dissociate cyclin D, indicating the formation of ternary INK4−CDK−cyclin D complexes (*23*). Thus, the conformation of p16 and p19 bound to CDK6, and the interactions revealed from the structures of the binary complexes, may not represent the corresponding information in the ternary complex. Second, even if the crystal structures of the binary complexes represent closely the functionally active forms, it is important to evaluate the quantitative contributions of specific residues to the inhibitory activity. This is a difficult task because the interactions between INK4 proteins and CDKs involve a large surface area. Third, different members of the INK4 family may show different specificity and binding affinity to CDK4/6. For example, it has been reported that p18 binds to CDK4 more weakly than to CDK6 (*24*), which suggests that INK4 proteins may have different specificity in vivo. Therefore, it is important to perform detailed structure−function analyses of different members of the INK4 family in order to understand the mechanism of binding and inhibition.

To date, information on the interactions of the ternary p16−CDK4−cyclin D complex has been obtained mainly from functional studies of p16 (*18*, *19*). The goal of this paper is to use site-specific mutagenesis and structural analyses to quantitatively evaluate the interactions between p18 and the preassembled CDK4−cyclin D2 complex. Since p18 is much more stable than p16 (*18*), most of p18 mutants retain unperturbed global structures, which enabled us to distinguish those functionally important residues from structurally important residues and quantitatively evaluate each potential interaction. The results can provide quantitative contributions of specific residues to the function of p16, and also address whether the presence of cyclin D affects the interactions between p16 and CDK4. The use of p18 also allowed us to address the second major goal of this work—to determine whether the additional ankyrin unit in p18 is involved in the interaction between p18 and the CDK4−cyclin D2 complex.

Our results suggest that p18 interacts with the preassembled CDK4−cyclin D2 complex in a similar way as predicted from the crystal structures of p16−CDK6 and p19−CDK6 binary complexes. However, there are significant differences in a few residues, suggesting that the interactions in the ternary complexes (in the presence of cyclin D2) may be different from the interactions in the binary complexes. Moreover, our results suggest that additional interactions at the extra loop of p18 could be required for the complete inhibition activity of p18, even though the crystal structure

of the p19−CDK6 complex indicates no interactions involving this loop.

MATERIALS AND METHODS

Construction and Purification of p16 and p18 Mutants. All p16 and p18 mutants were constructed in Quickchange method (Stratagene). pTG−p16 and pGEX−p18 were used as template for p16 and p18 mutants, respectively. All mutants were overexpressed and purified as described (*18*).

Assay for CDK4 Inhibition. CDK4−cyclin D2 holoenzyme and GST−pRb were made as described (*18*). The in vitro CDK4 inhibition reaction mixtures included 3−10 units of CDK4−cyclin D2 complex and varying amount of p16, p18, or their mutants in Kinase buffer (50 mM HEPES, pH 7.5, 10 mM $MgCl_2$, 2.5 mM EGTA, 0.1 mM Na_3VO_4, 1 mM NaF, 10 mM β-glycerophosphate, 1 mM DTT, 0.2 mM AEBSF, 2.5 mg/mL leupeptin, and 2.5 mg/mL aprotinin) in a total volume of 15.0 μL. The reaction mixture was kept at 30 °C for 30 min, then 50.0 ng of GST−pRb and 4.0 μCi of [γ-^{32}P]ATP were added into each mixture and the samples were incubated at 30 °C for an additional 15 min. The reaction was terminated by the addition of 5x SDS-PAGE loading buffer (*25*) into each mixture. ^{32}P-labeled GST-Rb was separated by SDS-PAGE, and quantitatively analyzed by Phosphorimager (Molecular Dynamics, Inc.).

^{15}N-Labeling. The uniform ^{15}N-labeled samples were prepared as follows: the bacteria (*Escherichia coli* BL 21, DE 3) was grown at 37 °C on a M9 minimal medium containing ^{15}N-ammonium sulfate at the concentration of 1.0 g/L as the only nitrogen source (*25*). When OD_{600} of the culture was around 0.9, the culture was chilled on ice for 10 min, and IPTG was added into the culture to the final concentration of 0.1 mM. The culture was grown at 25 °C for additional 24 h. Labeled proteins were purified in the same way as unlabeled mutants. The expression levels of wild-type p16 and p18 were about 15.0 mg/L, and some mutations may lead to low expression levels.

NMR Experiments. All NMR experiments were performed on a Bruker DMX-600 spectrometer at 20 °C as described previously (*18*). The concentration of proteins ranges from 0.2 to 0.4 mM. Protein samples for 1D and 2D NOESY NMR contained 4 mM HEPES buffer containing 1 mM DTT and 5 mM EDTA (pH 7.5) in 100% ^2H_2O, and that for ^{15}N−^{1}H HSQC was in the same HEPES buffer in 95% H_2O/5% ^2H_2O.

Guanidinium Chloride Titration of p18 Mutants. Samples containing 7.5∼10 μM proteins in 20 mM sodium borate buffer (pH 7.5) and 40 μM DTT were incubated with different amounts of guanidinium chloride on ice overnight, and then equilibrated at 19 °C just prior to CD analysis. The rotation at 220 nm was measured on a JASCO J-500C spectrometer, and the exact concentrations of guanidinium chloride were calculated using its refraction index. The concentration of guanidinium chloride at half-denaturation and the free energy of denaturation in water were obtained on the basis of two-state approximation (*26*).

Analyses of Interactions. Calculations were performed using Naccess V2.1.1−(Atomic Solvent Accessible Area Calculations) provided free from S. Hubbard and J. Thornton, using a 1.0 Angstrom probe radius. Other parameters used were as described in the software manuals. Values were then plotted using microsoft Excell.

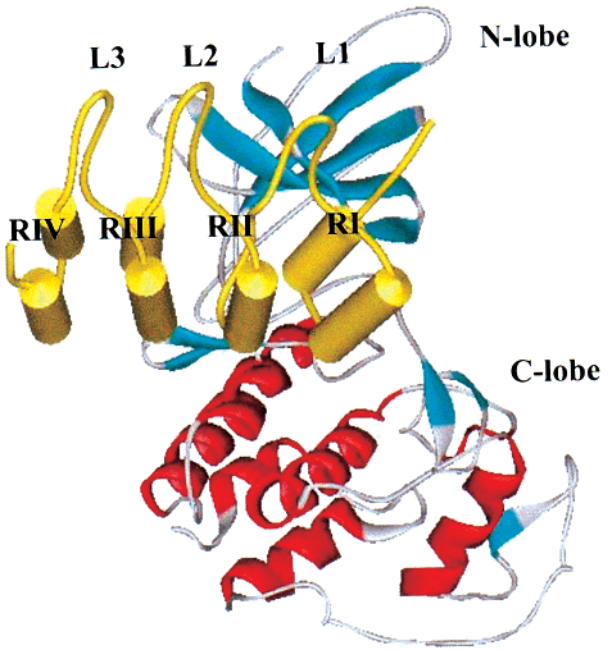

FIGURE 2: Crystal structure of the p16−CDK6 complex (*21*) showing the major regions of interaction. The p16 structure is shown in yellow and the ankyrin repeats are labeled as RI−RIV and the loops as L1−L3. The two helices of each ankyrin repeat are designated as A and B, which are labeled in Figure 1 but not in this figure. The figure is prepared with Web Lab Viewer Pro (MSI Inc.).

RESULTS AND DISCUSSION

Analyses of the Interactions in p16−CDK6 and p19−CDK6 Complexes. Although this paper focuses on p18 (the only member in the family with both crystal and solution structures of the free form reported), we start by analyzing the crystal structures of p16−CDK6 and p19−CDK6 binary complexes in detail for three purposes: to assist in the rational design of p18 mutants, to serve as a basis for comparison with the results of functional analyses, and to examine the difference between the two complexes.

As shown in the crystal structure of the p16−CDK6 complex (*21*) in Figure 2, there are three main regions of interaction between the two proteins. The first involves loops 1 and 2 (but not loop 3). Both loops 1 and 2 interact with CDK6 through the last 5−6 amino acids of the loop preceding the next ankyrin. The second interacting region involves the first helix (denoted helix A) in each set of helices that form an ankyrin repeat. The third major region of interaction is located at the "turns" in the helix-turn-helix motifs. The B helices, on the other hand, make very little contact with the kinase, as shown in the crystal structure.

Although the global folds and contacts of the two binary complexes are very similar, further analyses suggested that they differ in some specific interactions as well as in the surface area of the binding interface. In the p16−CDK6 complex well over 2200 Å^2 are involved in the interaction, whereas in the p19−CDK6 complex only 1700 Å^2 are in contact (*21*, *22*). A breakdown of the interaction by ankyrin repeat is shown in Figure 3. In both complexes, the interactions of ankyrin II has the largest surface area of contact with CDK6. The second largest contribution comes from ankyrin III. In this region, p16 shares more binding surface with CDK6 than does p19. It is of interest that

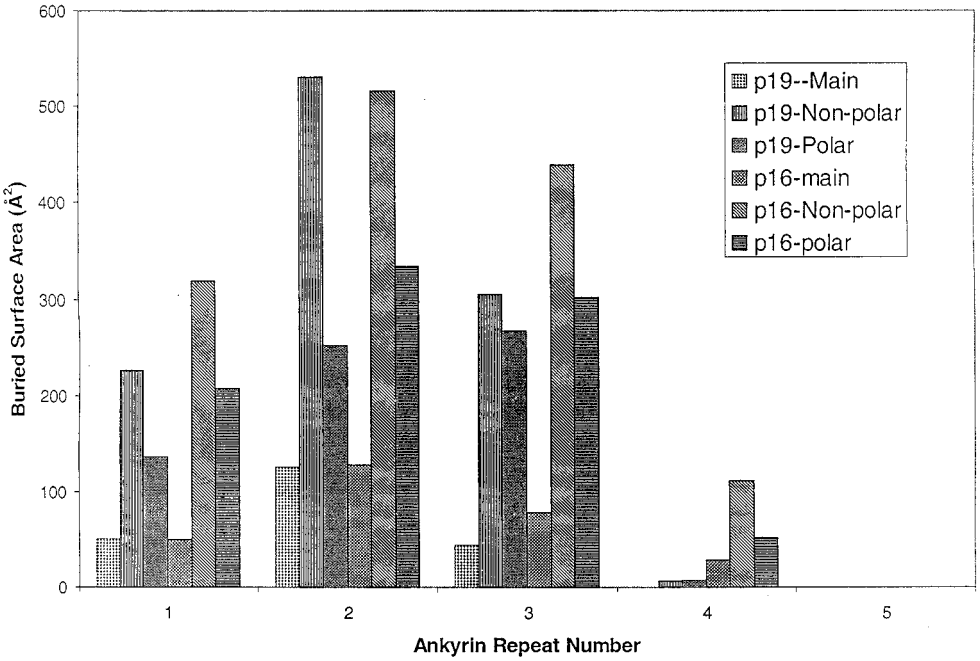

FIGURE 3: A breakdown of the types of interactions by ankyrin repeat for p16 and p19. Interactions are analyzed by polar, nonpolar and mainchain buried volume. Computations were performed with the program NACCESS v 2.1.1 (*29*)

ankyrin II contains the largest interacting surface, while the greatest sequence homology lies in ankyrin III. In the first and fourth ankyrin repeats p16 also has a larger buried surface area than p19. Indeed, in the fourth ankyrin repeat p19 is barely interacting. As for the fifth ankyrin that is shared between p18 and p19, there appears to be no interaction. This raises the issue why p18 and p19 contain the fifth ankyrin repeat.

The specific interactions between p16 and CDK6, and between p19 and CDK6, also show notable differences. Some of these differences are due to the fact that some of the surface residues in the two proteins have contrasting charges. For example, Arg24 of p16 corresponds to Asp20 in p19. In the p16−CDK6 complex Arg24 of p16 interacts with Asp104 and Thr106 of CDK6, while in the p19−CDK6 complex Asp20 interacts with Arg168 of CDK6. Such differences have been analyzed in detail elsewhere, in the context of all four INK4 proteins (*20*). Occasionally, differences in specific interactions arise where there is sequence identity between p16 and p19. For example, Glu27 of p16 forms a salt bridge with Arg168 of CDK6. p19 has a corresponding Glu residue (Glu23); however, it is Gln22 of p19, which interacts with Arg168 of CDK6.

The clearly discernible differences between p16−CDK6 interactions and p19−CDK6 interactions suggest that interactions between different INK4 proteins and CDKs are different in detail, and that such differences could contribute to the specificity of interactions.

Design and Construction of p18 Mutants. It is not the goal of this paper to evaluate all of the interactions in p16−CDK6 and p19−CDK6 complexes. In fact the system of this study differs from these two crystal structures in a few aspects: (i) since p19 and p16 interact somewhat differently with CDK6 as described in the previous section (*21*, *22*), p18 could also interact with CDKs differently; (ii) the CDK used in our study is CDK4, while that used in the crystal structures is CDK6; (iii) the functional analyses deal with the p18−CDK4−cyclin D2 ternary complex, while the crystal structures represent only binary complexes.

The goal of this work is to perform structure−function analyses on the inhibition of p18 to the preassembled CDK4−cyclin D2 complex. On the basis of the information available from related systems as described above, we designed a total of 24 mutants of p18, as shown in Table 1. These include 18 single mutants at various regions, four double mutants, one triple mutant, and one deletion mutant. The first mutant at a given position is always alanine mutant; in a few cases, additional mutants with drastic changes in the property of the side chain were constructed. The double and triple mutants were designed to further confirm the mutagenic effects on the inhibition. These mutants have all been expressed in *Escherichia coli* and purified to homogeneity.

The Conformations of Single and Double Mutants Are Not Perturbed. One-dimensional proton NMR experiments were first employed to characterize these mutants. Figure 4 shows the 1D NMR spectra of WT p18 (A), a representative single mutant R39A (B), a representative double mutant R133A/K136A (C), the triple mutant R68A−E102A−H135A (D), and the deletion mutant Δ133−136 (E). The corresponding 2D NOESY spectra are shown in Figure 5. The spectra of R39A and R133A−K136A are very similar to that of WT p18; the same is true for most of the other single and double mutants (not shown). These results are dramatically different from the results for p16 mutants where a single mutation often induced significant aggregation and/or conformational perturbations (*15*, *19*).

In addition, $^{15}N-^{1}H$ HSQC spectra of K136A (B) and R133A−K136A (C) were compared to that of WT p18 (A) (Figure 6). For K136A, the cross-peak corresponding to K136 disappears, while two other cross-peaks have detectable shifts. One cross-peak, corresponding to G137, is shifted by 0.7 ppm for ^{15}N, and the other one, corresponding to H135, is shifted by 0.1 ppm for ^{1}H. For R133A−K136A, more

Table 1: IC_{50} Values and Structural Properties of Mutants of p18

mutant	counterpart in p16	location	structural properties	IC_{50} (nM)
	WT			70 ± 25
WT				80 ± 20
R15A	R22	helix IA	retained	240 ± 40
E19A	E26	helix IB	retained	320 ± 30
E19R	E26	helix IB	retained	580 ± 80
F37A	Y44	loop 1	retained	320 ± 40
F37D	Y44	loop 1	retained	350 ± 40
R39A	R46	loop 1	retained	410 ± 60
R39E	R46	loop 1	retained	540 ± 80
D67A	D74	loop 2	retained	245 ± 20
R68A[a]	A76	loop 2	retained	250 ± 35
T69A[a]	T77	loop 2	retained	360 ± 50
T69L	T77	loop 2	retained	420 ± 70
D76A	D84	helix IIIA	retained	>3500
R79A	R87	helix IIIA	retained	100 ± 15
N101A	A109	loop 3	retained	170 ± 30
E102A	W110	loop 3	retained	150 ± 30
R133A	N141	loop 4	retained	290 ± 35
H135A	A143	loop 4	retained	310 ± 40
K136A	R144	loop 4	retained	420 ± 50
D67A/R79A	D74/R87	loop 2/H IIIA	retained	250 ± 30
R79A/D84A	R87/D92	helix IIIA/B	retained	190 ± 30
R133A/K136A		loop 4	retained	530 ± 50
E102A/H135A		loops 3,4	retained	320 ± 50
R68A/E102A/H135A		loops 2,3,4	retained	470 ± 60
Δ133−136		loop 4	retained	570 ± 70

[a] The data for these two mutants have been included in the previous paper (*18*).

cross-peaks have detectable shifts, but the shifts are less than 0.1 ppm for ^{1}H and 1.0 ppm for ^{15}N. Most of these cross-peaks correspond to loop 4 residues, including H132, R133, H135, N134, K136, G137, D138, and T139, and the residues at the flexible C-terminus (such as G162, A164, and T165). Overall, these three spectra are almost identical, except at the mutated residues. Taken together, these NMR results indicate that the global conformations of single and double mutants are not significantly perturbed.

Conformational Analysis of Triple and Deletion Mutants. The 1D ^{1}H NMR spectrum of the triple mutant R68A−E102A−H135A (Figure 4D) is also very similar to that of WT except that the nonexchanging NH protons at 8−9 ppm have mostly disappeared. The 2D NOESY spectrum (Figure 5D) shows the same. These results suggest that the global conformation of this mutant has not been perturbed, but that the conformational flexibility has increased. The deletion mutant Δ133−136, which loses four polar residues at loop 4, displayed 1D and 2D spectra (Figure 4E and 5E) very similar to those of WT p18, except that the signal/noise ratios are lower. This mutant probably is unstable, since the protein expression is comparatively low. However, it is unexpected that deletion of four residues at loop 4 does not disrupt the tertiary structure. To further confirm this, we performed CD experiments to quantitatively determine the conformational stability of p18 mutants by monitoring the denaturation induced by guanidinium chloride. As shown by the data listed in Table 2, R39A, R133A−K136A, R68A−E102A−H135A, and Δ133−136 behave very similarly to p18 WT in the values of $D_{1/2}$, $\Delta G_D H_2O$, and m, suggesting that these mutations do not cause significant changes in the conformational stability of p18.

In summary, most mutants examined have unperturbed structures. Therefore, changes in the inhibitory abilities can be attributed to the functional roles of the mutated residues. This is a significant improvement from our studies of p16 mutants in which the structures of many of the mutants were perturbed or could not be evaluated due to aggregation. In essence, this paper represents the first site-specific mutagenesis study of an INK4 protein in which the global conformations of the mutants have been carefully analyzed.

Functional Analysis of WT p18 and Mutants. The assays were performed as described previously for p16 (*18*). Examples of the inhibition of CDK4 activity by p18 and three mutants are shown in Figure 7. The IC_{50} values determined are summarized in Table 1. As shown in Table 1, WT p18 has an IC_{50} value almost identical to that of p16. Thus both proteins have comparable CDK4-inhibitory abilities in vitro. Increases in IC_{50} values of 2-fold or less, such as for N101A, E102A, and R79A are considered insignificant (*18*). All other mutants have elevated IC_{50} values of 3-fold or higher. The mutants with IC_{50} values increased by 5-fold or higher are E19R, R39A, R39E, T69L, D76A (largest, >43-fold), K136A, R133A−K136A, and Δ133−136 of p18.

Summary of the Results. Our results showed four important points: (a) as shown in Figure 8, the functionally important residues of p18 involve multiple regions, including the residues at the tip of loops 1 and 2 (but not loop 3), along with a few helix residues. This pattern is in general agreement with that of p16. However, there are some differences in specific interactions. (b) The effects on IC_{50} values are small for most mutants except D76A, which reflects the fact that a large number of residues are involved in the interaction. There are more mutants of p16 with higher IC_{50} values; however, the p16 mutants are more likely to be perturbed structurally (*18*, *19*). (c) A few key residues in the X-ray structures of the binary complexes are not functionally important. This suggests that the binary complex structure may not represent the functionally active state of the system. (d) Although the crystal structure of p19−CDK6 indicates that loop 4 is not involved in binding, our functional results suggest that it is as important as loop 1 and loop 2 in p18.

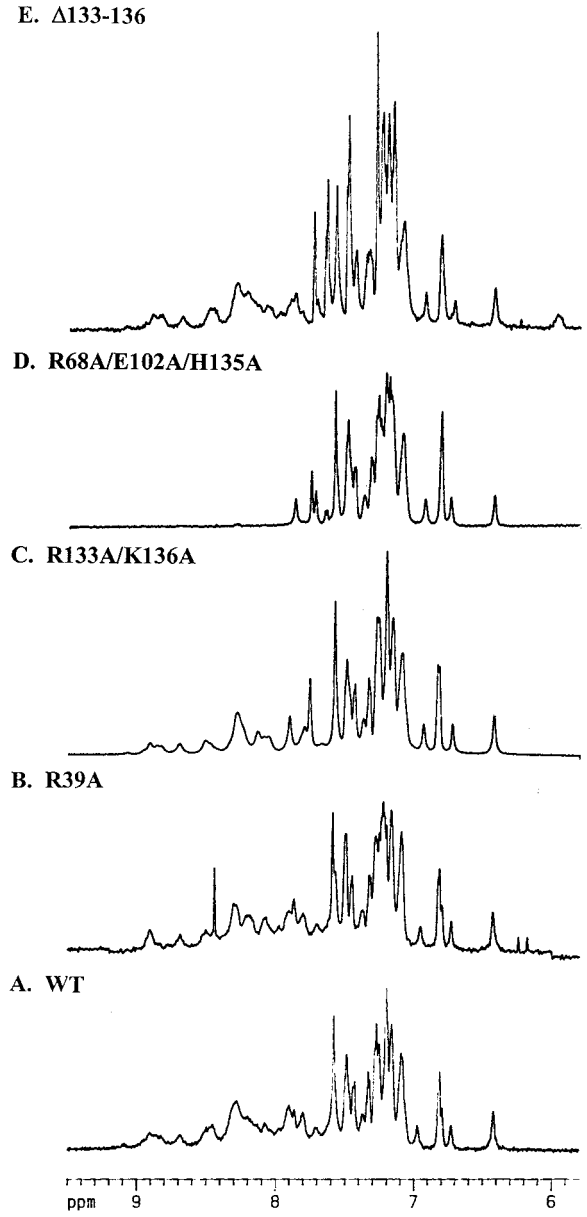

FIGURE 4: Comparison of partial 1D ^1H NMR spectra between WT p18 and representative mutants, in ^2H_2O at 600 MHz: (A) WT p18; (B) R39A; (C) R133A/K136A; (D) R68A/E102A/H135A; (E) Δ133−136. All samples were prepared in 4 mM HEPES/1 mM DTT/5 μM EDTA, pH 7.5, in D_2O. The NMR experiments were performed at 293 K.

Table 2: Conformational Stability of p18 WT and Mutants[a]

mutant	$D_{1/2}$ (M)	$\Delta G_D^{H_2O}$ (kcal mol^{-1})	m (kcal mol^{-1} M^{-1})
WT	0.9	2.78	3.15
R39A	1.0	2.73	3.14
R133A/K136A	0.9	2.74	2.97
R68A/E102A/H135A	0.8	2.98	2.79
D133−136	0.7	2.42	3.44

[a] $\Delta G_D^{H_2O}$, $D_{1/2}$, and m values were calculated according to a two-state model (*26*). The estimated error in such analyses is +/−5%.

This also supports the view that the binary complex structure may not represent the functionally active form of p18. In addition, it suggests that the interactions between different members of the INK4 family and different CDK (4 or 6) could all be slightly different, and that the differences could be important in controlling the specificity and the strength of binding. These points are further elaborated in the following sections.

Analyses of Interactions at Loops 1−3. Loop 1: In the crystal structure of the p16−CDK6 complex, loop 1 residues Y44 and R46 contact CDK6. Y44 has a hydrophobic interaction with F28 of CDK6 (corresponding to Y21 in CDK4), and R46 contacts E14 of CDK6 (E7 in CDK4) through an electrostatic interaction (*21*). The corresponding residue, K43 of p19, has also been found to form an electrostatic interaction with E14 of CDK6 (*22*). As shown in Table 1, mutations of each of these residues (F37A, F37D, R39A, and R39E in p18, corresponding to Y44A/D and R46A/E, respectively, in p16) led to increased IC_{50} values. The results suggest that loop 1 is involved in the interaction between p18 and CDK4/cyclin D. *Loop 2*: The results of p16 mutants suggested that loop 2 plays an important role in the interaction with CDK4 (*20*). For p18, we have mutated three polar residues at the tip of loop 2: D67A, R68A, T69A, and T69L. In the crystal structures of p16−CDK6, all three residues are in contact with CDK6 residues. As shown in Table 1, all four mutants show modest increases (3−5-fold) in the IC_{50} value. These results support the notion that loop 2 is involved in p18-CDK4 interactions. *Loop 3:* Although it has been suggested that loop 3 changes conformation upon binding of p19 to CDK6 (*22*), no significant interaction has been found between the loop 3 of p19 or p16 and CDK6 (*21*, *22*), with the exception of Trp110 of p16 which is involved in hydrophobic contacts with a few CDK6 residues. Our functional results suggest the same; mutations at the tip of loop 3 in p18 (N101A and E102A) did not bring about increases in IC_{50} values by more than a factor of 2. As shown in Figure 1, these two tip residues are not conserved among the INK4 family members. Residues N101 and E102 in p18 correspond to A109 and W110 respectively in p16, and G104 and T105 respectively in p19.

Analyses of Interactions at H-T-H Motifs. Although the second ankyrin appears to have a large area of interaction with CDK6 as shown in Figure 3, the first and third H-T-H motifs appear to have more conserved residues that are involved in specific interactions with CDK on the basis of the crystal structures of the binary complexes. Two mutants at the first H-T-H motif of p18 were constructed: R15A (corresponding to R22A in p16) and E19A (E26A in p16). As shown in Table 1, the IC_{50} values of both mutants increase by 3- to 4-fold. The IC_{50} value increases further to 7-fold for the E19R mutant. Even though such increases are modest, they are comparable to the increases caused by loop residue mutations and thus support the idea that both types of residues play a functional role.

The most important H-T-H motif is probably that of ankyrin III. A 20-residue peptide, encompassing residues 83−104 of p16, has been reported to bind to and inhibit CDK4 in tissue cultures (*27*). In p16−CDK6 and p19−CDK6 crystal structures (*23*, *24*), the third H-T-H motif is located at the interface between the inhibitor and the kinase. Mutagenesis studies of p16 have identified three important residues in the third H-T-H motif: D84, F90, and D92 (in p16 numbering). In this work, we constructed four mutants in this region of p18: D76A (corresponding to D84A in p16), R79A (R87A in p16), double mutant R79A−D84A (R87A−

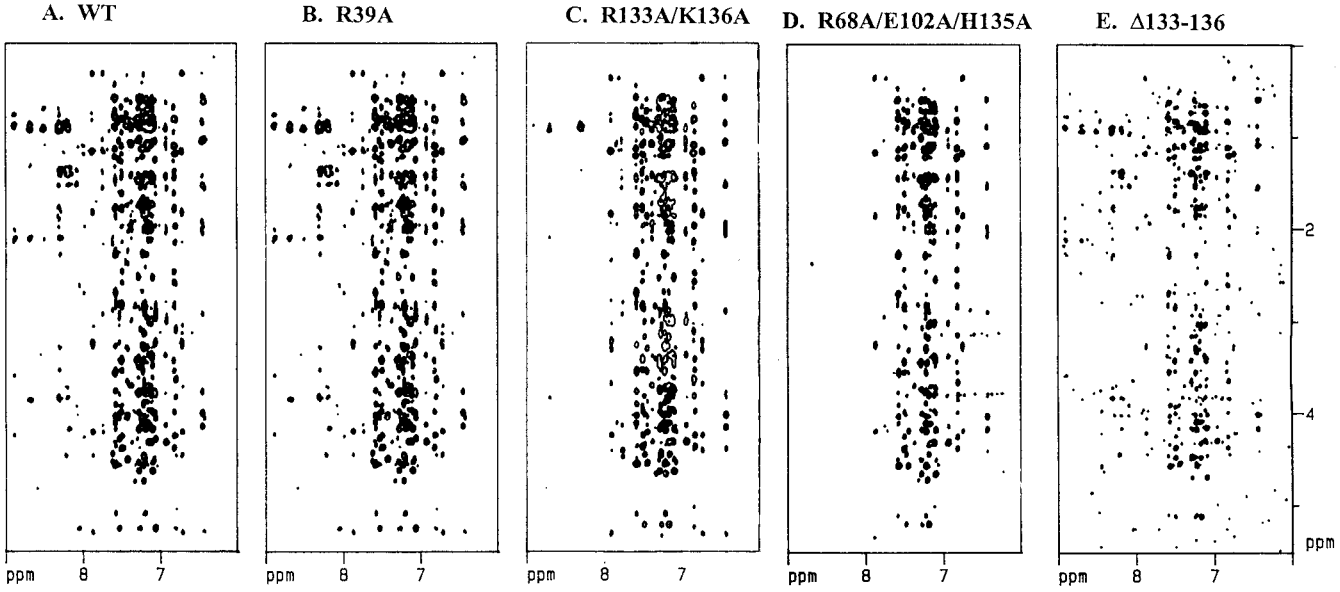

FIGURE 5: Comparisons of 2D NOESY NMR spectra between WT p18 and mutants, in ^2H_2O at 600 MHz: (A) WT p18; (B) R39A; (C) R133A/K136A; (D) R68A/E102A/H135A; (E) Δ133−136. The conditions are as described in Figure 4.

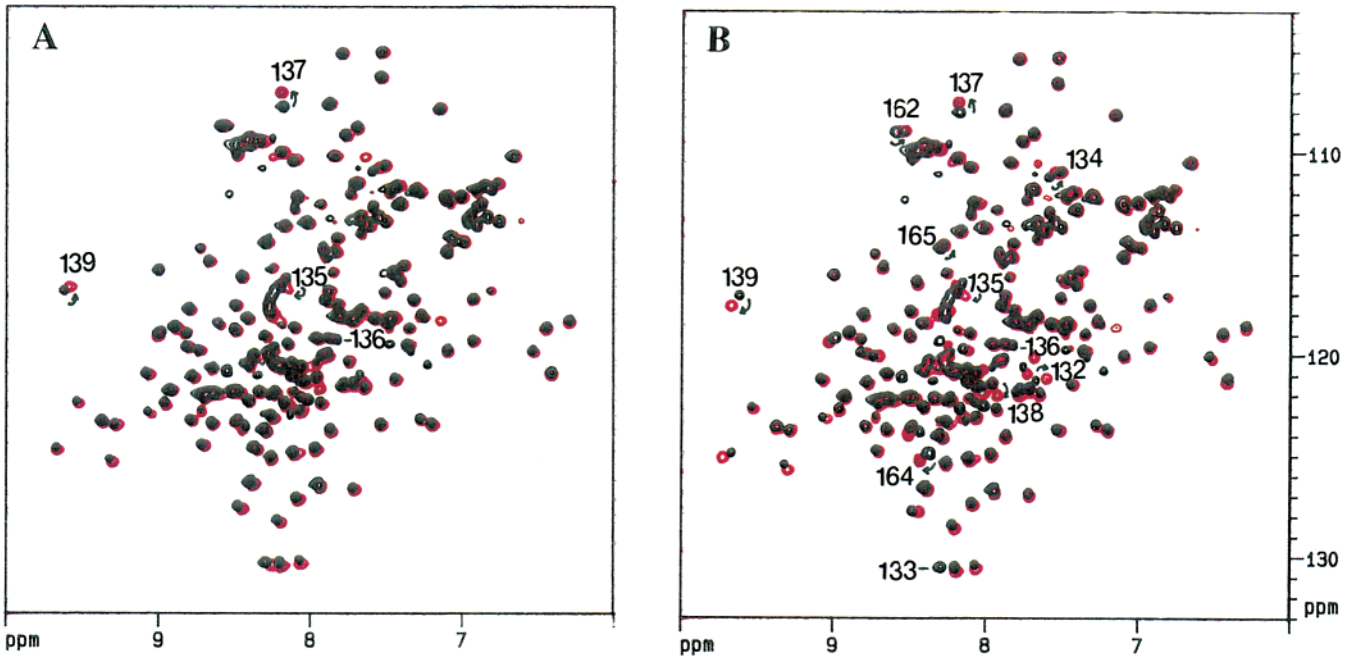

FIGURE 6: Comparisons of ^{15}N-^1H HSQC spectra of mutants with WT p18 in ^2H_2O at 600 MHz. A. K136A (red) and WT p18 (black); B. R133A/K136A (red) and WT p18 (black). The R133 and K136 peaks are labeled in the WT spectra that are missing in the K136A and R133A/K136A mutant spectra. The peaks that show larger chemical shifts are labeled with arrows.

D92A in p16), and double mutant R79A−D67A (R87A−D74A in p16). In the p16−CDK6 binary complex, D84 and D92 form electrostatic interactions with R31 and K111 of CDK6, respectively (corresponding to R24 and K106 in CDK4). Since R24 of CDK4 has been reported to play a key role in its kinase activity (*28*), the interaction between D84 of p16 and R24 of CDK4 is critical for the inhibition. As shown in Table 1, the alanine substitution of D76 in p18 (corresponding to D84 in p16) loses most inhibitory ability in vitro. However, both R79A and R79A−D84A in p18 show little increase in IC_{50} values, suggesting that these two residues do not contribute significantly to the inhibition. These results could imply differences between p16 and p18, and/or between binary complexes and ternary complexes, as discussed in the following sections.

Some Mutagenesis Results are Different from Those Revealed by Crystal Structures of Binary Complexes. In the p16−CDK6 complex, D74 (from loop 2) and D84 (helix IIIA) of p16 (corresponding to D67 and D76, respectively, in p18) both form salt bridges or hydrogen bonds with R31 of CDK6 (*21*). The same interactions are also seen in the p19−CDK6 complex. As mentioned above, the side chain of R31 of CDK6 is perhaps the most important in the interaction with INK4 proteins. The D76A mutation of p18 led to a >43-fold increase in the IC_{50} value as described above. However, the D67A mutation led to only a 3-fold increase. The results suggest that one of the interactions is substantially more important than the other.

As another example, the side chain of Arg87 of p16 interacts with backbone residues of CDK6 in the crystal

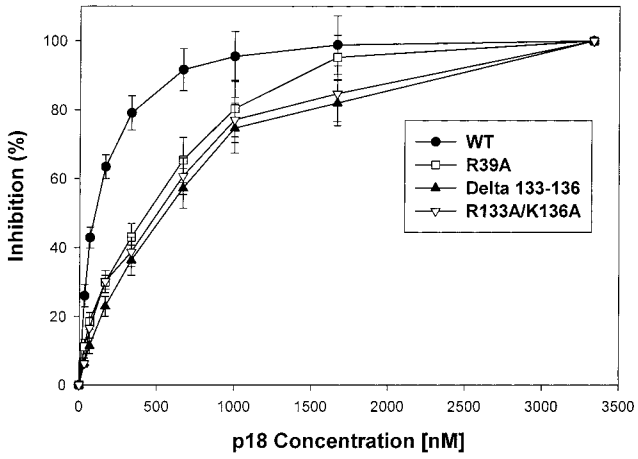

FIGURE 7: The in vitro CDK4 inhibition assay for WT p18, R39A, R133A/K136A, and Δ133−136. Inhibition curves were used to calculate the IC_{50} values. Measurements were repeated in triplicate.

structure of the binary complex (*21*). It also forms a salt bridge with Asp84 of p16. Thus one may predict that substituting this arginine with alanine will perturb the function of INK4 proteins. Unexpectedly, the R79A mutant of p18 (corresponding to R87A of p16) showed essentially the same activity as WT p18. One explanation for this apparent inconsistency is that the interaction between R87 in p16 and CDK6 is very weak. As we mentioned earlier, the structural studies do not provide a quantitative evaluation of all possible interactions, and it is reasonable that some interactions may contribute more to the inhibition than the others. An alternative explanation is that the interaction between INK4 proteins and the preassembled CDK4−cyclin D2 is different from that between INK4 proteins and CDK6 in the absence of cyclin D. A third possible explanation is that p18 interactions are different from p16 or p19 interactions.

Additional evidence suggesting that structures of binary complexes may not represent functionally active conformations comes from the results with loop 4 mutations, as discussed in the following section.

The Extra Loop of p18 Could Play a Functional Role. Single and double mutations as well as the deletion mutant, Δ133−136 at loop 4 clearly impair the inhibitory ability of p18, while no structural perturbation is introduced, suggesting that the last loop of p18 does play some functional role. However, in the crystal structure of the p19−CDK6 complex, no significant contact is formed between the extended portion of p19 (loop 4 and ankyrin V) and CDK6 (*21*). This difference may arise from (i) intrinsic differences between p18 and p19 or between CDK4 and CDK6, (ii) the presence of cyclin D2, and (iii) the dynamic nature of this inhibition process. While the specific causes remain to be established, our result represents the first evidence that p18 binds to the CDK4−cyclin D2 complex in a way different from the way in which p19 binds to CDK6 in the p19−CDK6 binary complex. The biological significance of this difference is still unknown, but we presume that this difference may contribute to the specificity of INK4 proteins.

While different members of the INK4 family clearly have different biological roles, it has not been established whether they have different mechanism of interactions with CDKs. Our analyses of surface charge (*20*) and buried areas (Figure 3) suggest that there are differences between p19−CDK6 interactions and p16−CDK6 interactions. The observation that loop 4 residues of p18 also contribute to the function of

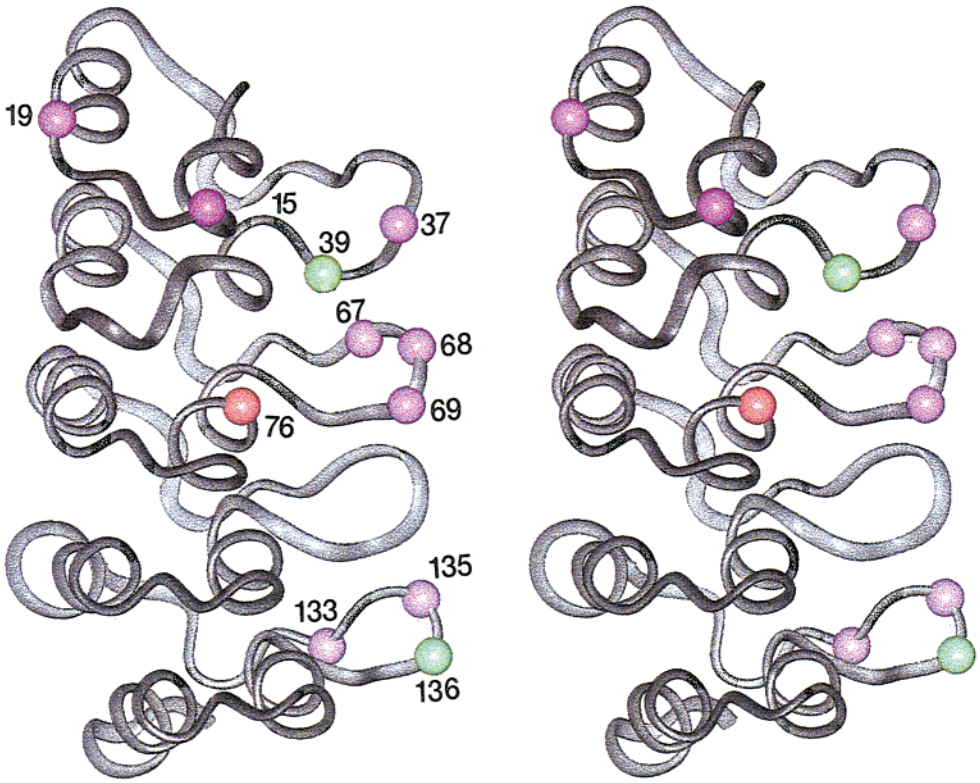

FIGURE 8: Contributions of functionally important residues of p18. The quantitative contributions of specific residues to the inhibition of CDK4 are indicated by color. If the alanine substitution of this residue causes the IC_{50} to increase by more than 20-fold, it is indicated by red (residue 76); 5−10-fold, green (residues 39 and 136); 3−5-fold, purple (residues 15, 19, 37, 67, 68, 69, 133, and 135).

p18 suggests that the mode of interactions of p18 is different from that of p16, since p16 does not have the extra loop.

Conclusion. While a large number of p16 mutants have been investigated, this paper presents the first in vitro study of p18 mutants. The more stable structural properties of p18 allowed more quantitative structure−function analyses. The results have uncovered significant information about p18−CDK4 interactions at the functional state (in the presence of cyclin D2), which are somewhat different from the interactions in p16−CDK6 and p19−CDK6 binary complexes. Most significantly, the extra loop of p18 appears to contribute to its function. There are also noticeable differences between different members of the INK4 family.

Our results imply that different members of the INK4 proteins could have different biological functions as well as different mechanisms, and that the static structures may not represent functionally active states of the INK4 proteins. The in vivo functions of INK4 proteins in cell cycle regulation could also be affected by other factors such as their biological targets (different CDKs) or the phosphorylation state of CDKs. After submission of this paper, another important paper (*30*) reported that only p16 can form stable complexes with both CDK4 and CDK6 in vivo, while other INK4 proteins can form stable complexes with CDK6 but associate only transiently with CDK4, which demonstrated that the INK4−CDK interaction differs from each other among INK4 family and CDK family in vivo. Therefore, it is necessary to perform thorough structure−function analyses for each member of the INK4 proteins for their specific interactions with different members of CDKs.

ACKNOWLEDGMENT

The authors gratefully acknowledge A. Showalter for critical review of the manuscript, J. Cloud for purifying GST-Rb, and P. O'Maille for help in preparing figures. The expression vector, pGEX-p18, was a generous gift from Dr. Hengming Ke at U. of North Carolina.

REFERENCES

1. Carnero, A., and Hannon, G. J. (1997). In *Cyclin Dependent Kinase (CDK) Inhibitors* (Vogt, P. K., and Reed, S. I., Eds.) pp 43−55, Springer, New York.
2. Chellappan, S. P., Giordano, A., and Fisher, P. B. (1997). In *Cyclin Dependent Kinase (CDK) Inhibitors* (Vogt, P. K., and Reed, S. I., Eds.) pp 58−103, Springer, New York.
3. Jeffrey, P. D., Russo, A. A., Polyak, K., Gibbs, E., Hurwitz, J., Massague, J., and Pavletich, N. P. (1995) *Nature 376*, 313−320.
4. Matsouka, M., Kato, J. Y., Fisher, R. P., Morgan, D. O., and Sherr, C. J. (1994) *Mol. Cell. Biol. 14*, 7265−7275.
5. Solomon, M. J. (1993) *Curr. Opin. Cell Biol. 5*, 180−186.
6. Gao, C. Y., and Zalenka, P. S. (1997) *BioEssays 19*, 307−315.
7. Serrano, M., Hannon, G. J., and Beach, D. (1993) *Nature 366*, 704−707.
8. Kamb, A., Gruis, N., Weaver-Feldhaus, J., Liu, Q., Harshman, K., Tavigian, S., Stockert, E., Day III, R., Johnson, B., and Skolnick, M. (1994) *Science 264*, 436−440.
9. Hannon, G. J., and Beach, D. (1994) *Nature 371*, 257−261.
10. Chan, F. K. M., Zhang, J., Cheng, L., Shapiro, D., and Winoto, A. (1995) *Mol. Cell. Biol. 15*, 2682−2688.
11. Hirai, H., Roussel, M. F., Kato, J.-Y., Ashumun, R. A., and Sherr, C. J. (1995) *Mol. Cell. Biol. 15*, 2672−2681.
12. Okuda, T., Hirai, H., Valentine, V. A., Shurtleff, S. A., Kidd, V. J., Lahti, J. M., Sherr, C. J., and Downing, J. R. (1995) *Genomics 29*, 623−30.
13. Serrano, M. (1997) *Exp. Cell Res. 237*, 7−13.
14. Bork, P. (1993) *Proteins 17*, 363−374.
15. Tevelev, A., Byeon, I.-J. L., Selby, T., Ericson, K., Kim, H.-J., Kraynov, V., and Tsai, M.-D. (1996) *Biochemistry 35*, 9475−9487.
16. Luh, F. Y., Archer, S. J., Domaille, P. J., Smith, B. O., Owen, D., Brotherton, D. H., Raine, A. R. C., Xu, X., Brizuela, L., Brenner, S. L., and Laue, E. D. (1997) *Nature 389*, 999−1003.
17. Venkataramani, R., Swaminathan, K., and Marnorstein, R. (1998) *Nature Struct. Biol. 5*, 74−81.
18. Li, J., Byeon, I.-J., Ericson, K., Poi, M. J., O'Maille, P., Selby, T., and Tsai, M. D. (1999) *Biochemistry 38*, 2930−2940.
19. Byeon, I.-J., Li, J., Ericson, K., Selby, T. L., Tevelev, A., Kim, H. K., O'Maille, P., and Tsai, M.-D. (1998) *Molecular Cell 1*, 421−431.
20. Selby, T. L., Yuan, C., Li, J., Byeon, I.-J., and Tsai, M.-D. (1999) submitted.
21. Russo, A. A., Tong, L., Lee, J., Jeffery, P. D., and Pavletich, N. P. (1998) *Nature 395*, 237−243.
22. Brotherton, D. H., Dganaraj, V., Wick, S., Brizula, L., Domaille, P. J., Volyanik, E., Xu, X., Parisin, E., Smith, B. O., Archer, S. J., Serrano, M., Brenner, S. L., Blundell, T. L., and Laue, E. D. (1998) *Nature 395*, 244−250.
23. Guan, K. L., Jenkins, C. W., Li, Y., O'Keefe, S. N., Wu, X. Y., Zariwala, M., Matera, A. G., and Xiong, Y. (1996) *Mol. Biol. Cell 7*, 57−70.
24. Lapointe, J., Lachance, Y., Labrie, Y., and Labrie, C. (1996) *Cancer Res. 56*, 4586−4589.
25. Sambrook, J., Fritsch, E. F., and Maniatis, T. (1989). *Molecular Cloning*. 18.51−18.54, Cold Spring Harbor Laboratory Press, New York.
26. Pace, C. N. (1986) *Methods Enzymol. 131*, 266−280.
27. Fåhraeus, R., Paramio, J. M., Ball, K. L., Lain, S., Lane, D. P. (1996) *Curr. Biol. 6*, 84−91.
28. Wölfel, T., Hauer, M., Schneider, J., Serrano, M., Wölfe, C., Klehmann-Hieb, E., De Plaen, E., Hankeln, T., Meyer Zum Buschenfelde, K. H., and Beach, D. (1995) *Science 269*, 1281−1284.
29. Hubbard, S. J., and Thornton, J. M. (1993), "NACCESS", Computer Program, Department of Biochemistry and Molecular Biology, University College London.
30. Parry, D., Mahony, D., Wills, K., and Lees, E. (1999) *Mol. Cell. Biol. 19*, 1775−1783.
31. Li, J., Byeon, I.-J. L., Poi, M. J., Ericson, K., Selby, T., O'Maille, P., Qin, D., and Tsai, M.-D., In *DNA Alterations in Cancer: Genetic and Epigenetic Changes*, Melanie Ehrlich, Ed., BioTechniques Books, Eaton Publishing, in press (1999).

BI991281U